Marine and Petroleum Geology 110 (2019) 463–471

Contents lists available at ScienceDirect

Marine and Petroleum Geology

journal homepage: www.elsevier.com/locate/marpetgeo

Research paper

Influencing factors and fracability of lacustrine shale oil reservoirs

Cunfei Ma[a,b,c,d,e,*], Chunmei Dong[a,b,c,d], Chengyan Lin[a,b,c,d], Derek Elsworth[f], Guoqiang Luan[a], Xiaolong Sun[a], Xiaocen Liu[a]

[a] School of Geosciences in China University of Petroleum (East China), Qingdao 266580, China
[b] Key Laboratory of Deep Oil & Gas Geology and Geophysics (China University of Petroleum), Ministry of Education, Qingdao 266580, China
[c] Reservoir Geology Key Laboratory of Shandong Province (East China), Qingdao 266580, China
[d] Research Laboratory of China University of Petroleum (East China), Key Laboratory of Oil and Gas Reservoir of China National Petroleum Corporation, Qingdao 266580, China
[e] Key Laboratory of Shale Oil and Gas Exploration & Production, SINOPEC, Dongying 257100, China
[f] The Pennsylvania State University (University Park), State College, PA 16803, USA

ARTICLE INFO

Keywords:
Lacustrine shale oil
Fracability
Rock mechanics parameters
Influencing factors
Brittleness index

ABSTRACT

Shale oil reservoirs need fracturing in order to achieve commercial productivity. A key factor influencing the fracturing process is shale fracability, which is strictly dependent on rock fabric. In this study, we focused on the lacustrine shale oil reservoirs located in Dongying Sag and in the Northern Jiangsu Basin. Through X-ray mineral diffraction, rock mechanics, and P- and S-wave velocity tests, we analyzed the mineral components and mechanics of different shale lithofacies, as well as the influence of these factors on shale fracability. Based on the results of these analyses, we proposed a new method for the evaluation of lake shale oil reservoir fracability. The experimental results showed that the macrostructure, mineral content, lithology, and the presence of microfractures in the shale are the main factors affecting its brittleness. Shales with lamellar and sheet-like structures have relatively high Young's modulous or lower Poisson's ratios; under these conditions, netted fractures are easily formed during fracturing. The fracture toughness of carbonate minerals in shales is strong. An appropriate amount of carbonate minerals seemed to increase the shale brittleness; however, an excessive amount increased its cohesiveness, hindering the initiation and propagation of fractures. Felsic minerals are characterized by high brittleness, a characteristic that favors shale fracability; on the other hand, clay minerals and organic matter are highly plastic, a characteristic that hinders fracturing transformations. Due to their macrostructure and composition, lamellar clayey limestones (dolomite), lamellar clayey siltstones, layered calcareous (dolomitic) siltstones, sheet-like clay-containing siltstones, and flaggy carbonate-containing siltstones are expected to be easily fractured. In addition, the presence of microfractures seemed to reduce the overall fracture toughness of the rock: they penetrated artificial fractures, enhancing rock fracability. Taking into account the fracture toughness of carbonate minerals and the plastic effect of organic matter, we proposed a new formula for the calculation of the brittleness index, based on the mineral component method. The brittleness indices obtained through the proposed formula were linearly correlated with those calculated through the rock mechanics parameters method. Overall, our results indicate that the silty lithological successions occurring in the study area should be the easiest to fracture, followed by the calcareous (dolomitic) and clayey or organic-rich lithological successions. This study is of guiding significance for evaluating the fracability of different lithofacies in lacustrine shale oil reservoirs. Especially, the new proposed brittleness index containing the plastic effect of organic matter can correctly evaluate the actual brittleness of organic-rich shale.

1. Introduction

Shale oil reservoirs have very poor physical properties and flow ability. Hence, the application of fracturing techniques is necessary in order to connect matrix porosity and reach commercial productivity (Sheng and Li, 2016). For this reason, fracability is a key aspect to consider in shale oil reservoir evaluations (Chong et al., 2010). Many factors can affect shale fracability, including sedimentary structures, mineral components, mechanical properties, the presence of microfractures, diagenesis, and in-situ stresses (Breyer et al., 2010; Mullen

* Corresponding author. School of Geosciences in China University of Petroleum (East China), Qingdao 266580, China.
E-mail address: mcf-625@163.com (C. Ma).

https://doi.org/10.1016/j.marpetgeo.2019.07.002
Received 28 March 2019; Received in revised form 27 June 2019; Accepted 1 July 2019
Available online 02 July 2019

and Enderlin, 2012; Tang et al., 2012; Zhao et al., 2015; Zhuang et al., 2016; Wu et al., 2018). Among these factors, shale fabric and mechanical properties are probably the most important. A commonly applied indicator of shale fracability is the brittleness index, which is calculated based on the mineral component and rock mechanics parameters methods.

The mineral component method uses X-ray whole-rock mineral diffraction to quantify brittle and plastic mineral components to complete the quantitative calculation. This method, as originally proposed by Jarvie et al. (2007), considers quartz as the only brittle mineral: the higher the relative quartz content of a rock, the higher its brittleness. Afterwards, additional minerals have been included in the group of brittle minerals (e.g., dolomite, calcite, feldspar, mica), while the only plastic minerals considered until this moment have been clay minerals (Wang and Gale, 2009; Guo and Guo, 2013; Li, 2013; Jin et al., 2014; Hao et al., 2016). Therefore, scholars dispute the types of brittle minerals and neglect the plastic effect of organic matter (Yasin et al., 2017).

The brittleness index, proposed by Honda and Sanada (1956), was first calculated based on the rock hardness and bulk modulus. Later on, other scholars started to include the rock compressive strength, tensile strength, and fracture toughness (obtained from rock mechanics tests) in the calculation of rock brittleness (Hucka and Das, 1974; Lawn and Marshall, 1979; Andreev, 1995; Quinn and Quinn, 1997; Deng et al., 2013; Zhao et al., 2015, 2017; Yuan et al., 2017; Kivi et al., 2018). Based on the results of a series of rock mechanics tests on the Barnett Shale, Rickman et al. (2008) used the normalized Young's modulus and the Poisson's ratio to predict the brittleness index. The Young's modulus and the Poisson's ratio of a rock are usually derived from acoustic and density logging data (Yuan et al., 2013; Liu and Sun, 2015; Chekhonin et al., 2018). The method described above, however, has regional limitations; hence, a different prediction model needs to be establish for each locality, depending on the corresponding geological conditions. A series of stress-strain curves can be obtained through the rock mechanics tests. The peak shear strength, peak strain, residual shear strength, and residual strain described by the curves have been applied to the calculation of rock brittleness (Bishop, 1967; Beugelsdijk et al., 2000; Hajiabdolmajid and Kaiser, 2003; Goodway et al., 2010; Zhou et al., 2014; Wu, 2015; Kivi et al., 2018).

The lacustrine shale oil reservoirs in Dongying Sag and in the Northern Jiangsu Basin are the focus of this paper. We performed X-ray mineral diffraction, rock mechanics, and P- and S- wave velocity tests to obtain the mineral composition and mechanics parameters of different shale lithofacies; additionally, we analyzed the influence of rock fabric and microfractures on shale oil reservoir fracability. Based on the results of our analyses, we proposed a new method for the evaluation of lacustrine shale oil reservoir fracability.

2. Overview of the study area

The Jiyang Depression belongs to a first-order tectonic unit of the Bohai Bay Basin (eastern China). This depression borders with the Tanlu fault zone to the west, the Chengning uplift to the south, and the Luxi uplift to the north; additionally, it extends longitudinally (W-E) and latitudinally (N-S) over 240 km and 130 km, respectively, covering an area of 26 000 km^2. It represents a Mesozoic-Cenozoic fault-depression composite basin, which developed from the North China Platform, and includes four negative secondary tectonic units (i.e., Dongying Sag, Huimin Sag, Zhanhua Sag, and Chezhen Sag), plus a series of positive secondary tectonic units (i.e., Gudao uplift, Yihezhuang uplift, Chenjiazhuang uplift, Wudi uplift, Binxian uplift, and Kendong Qingtuozi uplift): the typical tectonic framework includes depressions alternated with uplifts (Fig. 1a). The Northern Jiangsu Basin corresponds to the land-based part of the Northern Jiangsu-South Yellow Sea Basin, located to the north of the Yangtze River (Jiangsu Province), and covers an area of ~3.5 × 10^4 km^2. The basin borders with the Lusu uplift to the north, the Zhangbaling uplift to the south, the Tanlu fault to the west, and the Yellow Sea to the east. Moreover, it represents a Mesozoic-Cenozoic continental basin that developed on the Lower Yangtze activated platform and consists of four sag basins: from east to west, we found the Haian, Gaoyou, Jinhu, and Yancheng sags (Fig. 1b).

The Paleogene Funing Formation (in the Northern Jiangsu Basin), as well as the Shahejie Formation (in the Dongying Sag) and the Zhanhua Sag (in the Jiyang Depression), were all formed during a fault-depression tectonic cycle. The second member of the Funing Formation (in the Northern Jiangsu Basin) is located within the transgressive systems tract of a secondary sequence, while the upper part of the fourth member and the lower part of the third member of the Shahejie Formation (in the Jiyang Depression) are located within the highstand systems tract of a lake. Nevertheless, all of them belong to a complete third-order sequence. Due to the continuous subsidence and to the injection of terrigenous clasts, the Northern Jiangsu Basin and Jiyang Depression contains abundant organisms and lacustrine sediments. During a period of intense fault-depression activity, thick and dark shales deposited in a deep-lake environment, characterized by semi-saline, weakly alkaline, and strongly reductive conditions. The second member of the Funing Formation, the upper part of the fourth member, and the lower part of the third member of the Shahejie Formation are represented by thin shale interbeds with different lithologies.

3. Research methods

3.1. Shale lithofacies determination

Currently, the most used method for the classification of shale lithofacies is based on the main mineral components of rocks (James and Bo, 2007; Mohamed and Roger, 2012; Wang, 2012). This method considers three main groups of minerals including carbonate, felsic, and clay minerals, and several internal subdivisions, following a three-level naming principle (Wang and Timothy, 2013). Based on these principles, we classified the shale lithofacies considering both their macrostructures and lithological characteristics. Shale macrostructures were determined by core observation, while their lithology was reconstructed through the identification of felsic (silt), clay, and carbonate minerals applying X-ray diffraction, as well as by whole-rock and thin-section observations (Dong et al., 2015).

3.2. The volume fraction calculation of organic matter

The total organic carbon content of shale is determined by organic carbon analysis. The volume fraction of organic matter is obtained by using the total organic carbon content, conversion coefficient, organic matter density and rock density. The calculation formula is as follows (Equation (1)).

$$V_o = W_o \times K \times \rho_m/\rho_o \quad (1)$$

where V_o is the volume fraction of organic matter, %; W_o is the total organic carbon content, %; K is the conversion coefficient of organic matter to organic matter content determined by the type of organic matter and the stage of diagenetic evolution (Table 1; Tissot and Welte, 1978); ρ_m is the density of shale, g/cm^3; ρ_o is the density of organic matter, g/cm^3.

3.3. Determination of shale static mechanics parameters

Rock static mechanics parameters are usually measured performing stress-strain experiments, which provide the elastic modulous E, μ, K, and the Poisson's ratio of the sample. We performed a series of stress-strain tests using a full servo-controlled triaxial test system (TAW-1000) owned by the Seismic Petroleum Physics Laboratory (China University of Petroleum, China). Following meticulously the method recommended by the International Society of Rock Mechanics, we

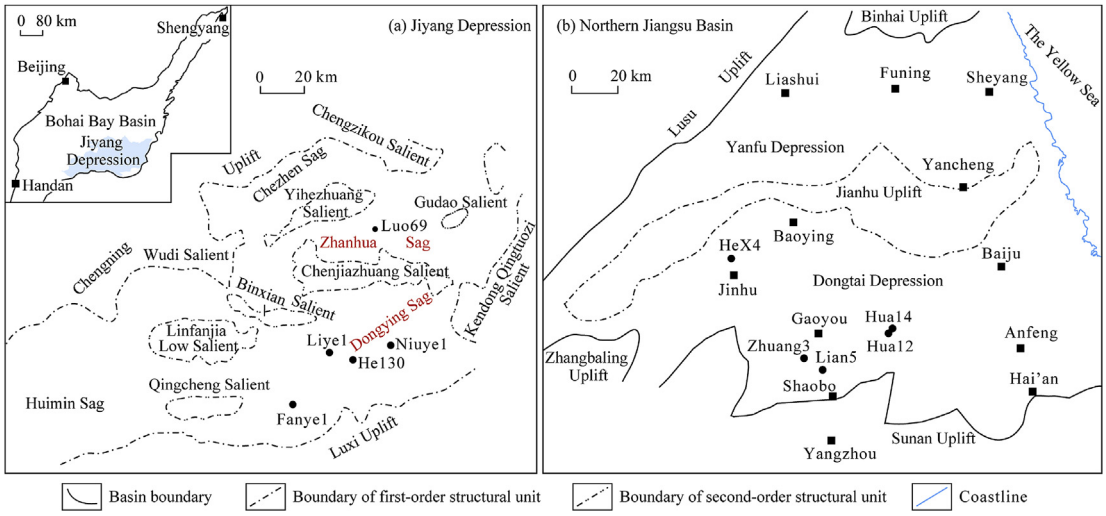

Fig. 1. Geological map of the study area.

Table 1
The conversion coefficient of organic matter.

Evolution stage	Kerogen type			Coal
	I	II	III	
diagenetic stage	1.25	1.34	1.48	1.57
plutonic stage	1.2	1.19	1.18	1.12

processed the sandstone samples, performed several stress-strain tests under different conditions, and processed the results. A series of triaxial mechanical tests according to the actual geological conditions of the study area: under high confining pressure, using horizontal and vertical rock samples. From these tests we obtained the rock compressive strength, static Young's modulus, static Poisson's ratio, internal friction angle, and cohesion (Table 2). The static Young's modulous of the shale samples from the study area ranged between 6.8 and 34.2 Gpa (average = 16 GPa), the static Poisson's ratio between 0.1 and 0.28 (average = 0.19), the compressive strength under high confining pressure between 63.6 and 390 Mpa (average = 167.5 Mpa); the internal friction angle between 15.7 and 26.5° (average = 19.9°), and the cohesive force between 11.7 and 49 Mpa (average = 34.9 Mpa) (Table 2).

3.4. Determination of the shale dynamic mechanics parameters

The HF-G Intelligent Ultrasound P.S Wave Comprehensive Tester, owned by the Seismic Petroleum Physics Laboratory (China University of Petroleum, China), can test the effects of P- and S-waves in rocks under the same conditions; this ability removes the need of

Table 2
Static shale mechanics parameters in the study area.

Lithofacies	Sample direction	Confining pressure/Mpa	Density /(g/cm^3)	Compressive strength/Mpa	Static Young's modulus/Gpa	Static Poisson's ratio	Internal friction angle/°	Cohesion/Mpa
sheet-like clay-containing siltstone	horizontal	70	2.7	287	26	0.12	\	\
sheet-like silty clay rock	horizontal	57	2.3	168.6	11.5	0.1	\	\
flaggy dolomite-containing siltstone	vertical	65	2.4	159.8	11.5	0.12	\	\
flaggy dolomite-containing siltstone	horizontal	65	2.6	211.5	22.3	0.22	\	\
lamellar clayey siltstone	horizontal	63	2.7	225.2	22.9	0.25	\	\
lamellar clayey siltstone	vertical	63	2.7	390	25.9	0.28	\	\
flaggy dolomitic clay rock	vertical	15	2.4	133.7	14.3	0.17	21.3	39.8
flaggy dolomitic clay rock	vertical	53	2.4	177.3	13.3	0.25	21.3	39.8
flaggy dolomitic clay rock	vertical	15	2.4	143	11.9	0.26	26.5	36.7
flaggy dolomitic clay rock	vertical	54	2.4	206	12.7	0.19	26.5	36.7
flaggy silty clay rock	vertical	15	2.4	90	8.6	0.23	17.8	27.8
flaggy silty clay rock	vertical	57	2.4	121	12.2	0.24	17.8	27.8
layered clayey siltstone	horizontal	15	2.3	138	10.2	0.22	19.4	43.5
layered clayey siltstone	horizontal	60	2.3	183	6.8	0.23	19.4	43.5
layered silty clay rock	vertical	10	2.5	70	8.9	0.12	20.7	11.7
layered silty clay rock	vertical	55	2.5	134	11.7	0.12	20.7	11.7
layered dolomitic clay rock	vertical	15	2.3	106	10.3	0.15	17.9	33.5
layered dolomitic clay rock	vertical	65	2.3	149	11.9	0.16	17.9	33.5
sheet-like clay-containing siltstone	vertical	45	2.3	153.4	9.4	0.2	\	\
lamellar clayey dolomite	horizontal	20	2.5	249.3	34.2	0.22	19.9	49.0
lamellar clayey dolomite	horizontal	0	2.6	106.5	32.7	0.19	19.9	49.0
layered calcareous siltstone	horizontal	0	2.4	63.6	15	0.1	15.7	37.5
layered calcareous siltstone	horizontal	30	2.4	186.8	24.6	0.22	15.7	37.5

Table 3
Dynamic shale mechanics parameters in the study area.

Lithofacies	Sample direction	Density /(g/cm^3)	P-wave velocity/(m/s)	S-wave velocity/(m/s)	Dynamic Young's modulus/GPa	Dynamic Poisson's ratio
layered clayey siltstone	vertical	2.6	4582	3436	52.65	0.14
layered clayey siltstone	horizontal	2.6	5290	3613	72.15	0.06
sheet-like clay-containing siltstone	horizontal	2.7	5276	3677	75.04	0.03
sheet-like silty clay rock	horizontal	2.3	3874	2788	34.43	0.04
flaggy dolomite-containing siltstone	vertical	2.7	4149	3084	45.33	0.12
flaggy dolomite-containing siltstone	vertical	2.4	4292	2877	43.39	0.09
flaggy dolomite-containing siltstone	horizontal	2.6	4552	2712	46.85	0.22
lamellar clayey siltstone	horizontal	2.7	5122	3688	70.63	0.04
lamellar clayey siltstone	vertical	2.7	5298	3637	75.31	0.05
layered dolomitic clay rock	vertical	2.5	3685	2468	33.30	0.09
layered dolomitic clay rock	horizontal	2.5	4250	2833	44.15	0.10
flaggy dolomitic clay rock	vertical	2.4	3830	2421	32.84	0.17
flaggy dolomitic clay rock	vertical	2.4	4197	2728	40.52	0.13
flaggy silty clay rock	vertical	2.4	4427	3018	46.60	0.07
layered clayey siltstone	horizontal	2.3	3937	2917	34.89	0.11
layered silty clay rock	vertical	2.5	4146	2393	35.80	0.25
layered dolomitic clay rock	vertical	2.3	4128	2893	39.17	0.02
sheet-like clay-containing siltstone	vertical	2.3	3342	2169	24.59	0.14
sheet-like silty clay rock	vertical	2.6	4887	3113	58.38	0.16
sheet-like silty dolomite	vertical	2.1	5178	3614	56.23	0.03
layered clayey dolomite	vertical	2.4	4994	3204	56.68	0.15

withdrawing temperature and pressure when the test is performed under boundary conditions (high temperature and high pressure). The P- and S-wave excitation systems are based on the propagation characteristics of ultrasounds in solids: they are equipped with special transducers and an innovative computer technology, which can test the passage of P- and S-waves in rocks and other non-metallic specimens without changing the clamping state and the coupling boundary conditions, and quantitatively recording the attenuation of the first wave amplitude. The results of the P- and S-wave measurements on the horizontal and vertical shale samples are shown in Table 3.

Based on the elasticity theory, the dynamic Young's modulus and the Poisson's ratio can be obtained using the P, S, and density experimental data, as in the following formulas (Equations (1) and (2); Gui and Wang, 2012).

$$V_d = \frac{0.5(\Delta t_s/\Delta t_c)^2 - 1}{(\Delta t_s/\Delta t_c)^2 - 1} \quad (2)$$

$$E_d = \frac{\rho_b(1 - 2V_d)(1 + V_d)}{\Delta t_c^2(1 - V_d)} \quad (3)$$

where V_d is the dynamic Poisson's ratio; E_d is the dynamic Young's modulus, Gpa; Δt_c is the P-wave time difference calculated from the reciprocal of P-wave velocity, s/m; Δt_s is the S-wave time difference calculated from the reciprocal of S-wave velocity, s/m; ρ_b is the volume density, g/cm^3.

In practical applications, array acoustic and density logging information can be used to obtain the necessary data when no P-wave, S-wave, or density testing data are available (Oyler et al., 2010; Yuan et al., 2013; Liu and Sun, 2015). In the study area, the shale density ranged between 2.1 and 2.7 g/cm^3 (average = 2.5 g/cm^3), P-wave velocity between 3342 and 5298 m/s (average = 4350 m/s), and S-wave velocity between 2169 and 3688 m/s (average = 2940 m/s) (Table 3). According to equations (2) and (3), the dynamic Young's modulus ranged between 24.6 and 75.3 Gpa (average = 45.8 Gpa) and the dynamic Poisson's ratio between 0.02 and 0.25 (average = 0.11) (Table 3).

4. Discussion

4.1. Characteristics of rock fabric

In terms of rock composition, the shale has polygenetic fine-grained felsic minerals (silt or very fine silt), clay minerals, carbonate minerals and organic matter with typical characteristics of fine grained, mixed, temperature-pressure sensitive and fluid active. The clastic grains in shale are not irregularly mixed together, but are generally arranged parallel to the layers in the rock structure, showing three types of bedding types: sheet-like, directional and massive. Specially, sheet-like bedding developing in the sheet-like shale lithofacies shows fine interbedding of argillaceous, calcareous layer or organic rich layers, and the lamina interface is clear, straight and continuous. Directional bedding developing in the lamellar shale lithofacies has the characteristics of directional arrangement or strip distribution of argillaceous, carbonaceous, organic, bioclastic or terrigenous clasts, and the interfacial layers are intermittent or not obvious. Massive bedding developing in the flaggy and layered shale lithofacies is characterized by uniform distribution or indistinct directional arrangement of components. In addition, there are many types of microfractures in shale, such as the structural fracture, bedding fracture and natural fluid pressure fracture.

4.2. Effects of rock fabric on shale fracability

4.2.1. Macrostructure

The distribution pattern of mineral components was determined by the shale macrostructure. Mineral components in lamellar and sheet-like structures were continuously or intermittently interbedded, with an alternation of brittle and plastic components. The above two factors enhanced the heterogeneity of rock physical properties and tended to concentrate stress; additionally, they facilitated the cracking of the bedding surface. Oriented and/or evenly distributed mineral components in flaggy and layered structures promoted an even distribution of stress and strain, minimizing the chances of rock cracking. Therefore, the macrostructure of a shale seems to affect its mechanics parameters: shales with lamellar and sheet-like structures were characterized by higher Young's modulous or lower Poisson's ratios, conditions which are favorable to the formation of reticulated fractures and to the cracking of flaggy or layered structures. Notably, flaggy and layered structures were normally effective in dispersing and absorbing external stress or strain, and hence difficult to crack (Fig. 2).

4.2.2. Rock components

Minerals are the basic components of rocks: their type and amount considerably affect the mechanical properties of a rock. The fracture toughness of carbonate minerals was high, meaning that they had a

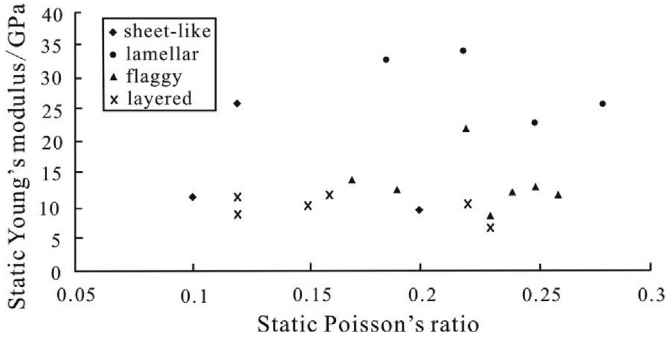

Fig. 2. Influence of shale macrostructure on the static Young's modulus and Poisson's ratio.

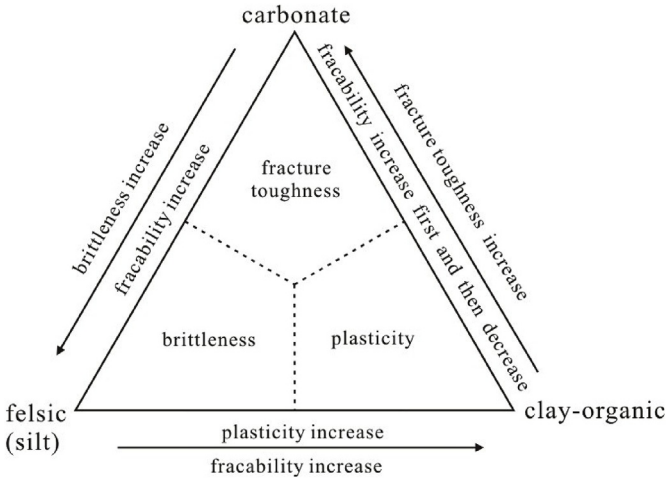

Fig. 3. Mechanical properties of different rock components and their influences on rock fracability.

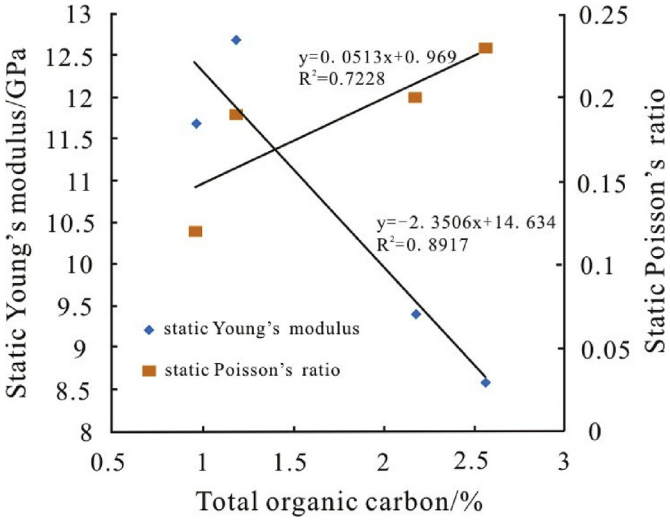

Fig. 4. Influences of total organic carbon on the static Young's modulus and Poisson's ratio of shale.

relatively high strength and a certain plasticity. An appropriate amount of carbonate minerals in the rock increased its brittleness, while an excess resulted in high rock cohesion, hindering fracture initiation and propagation: a high fracture toughness tended to lower rock fracability (Fig. 3). Felsic minerals had high brittleness, reflected by a moderate strength and low plasticity; hence, the presence of felsic minerals in a rock seems to increase its fracability (Fig. 3). On the other hand, clay

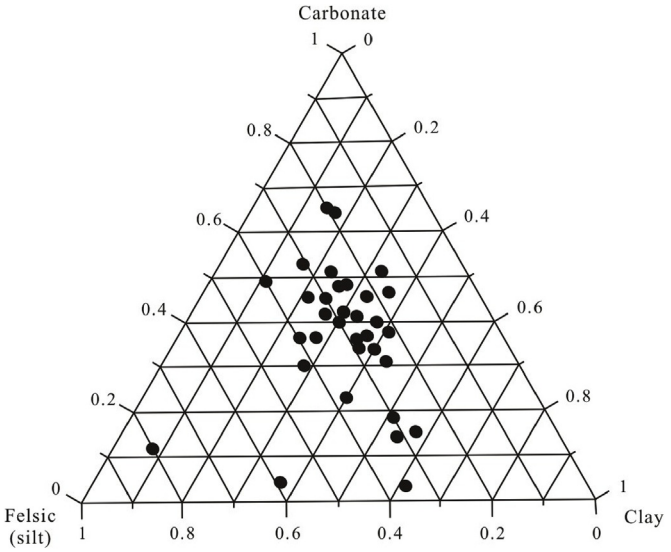

Fig. 5. Triangular map of mineral composition of shale with structural fractures.

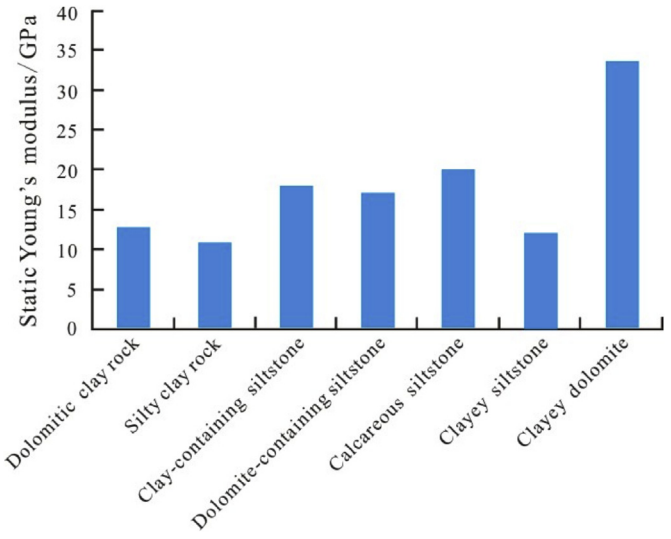

Fig. 6. Static Young's modulus of different shale lithologies.

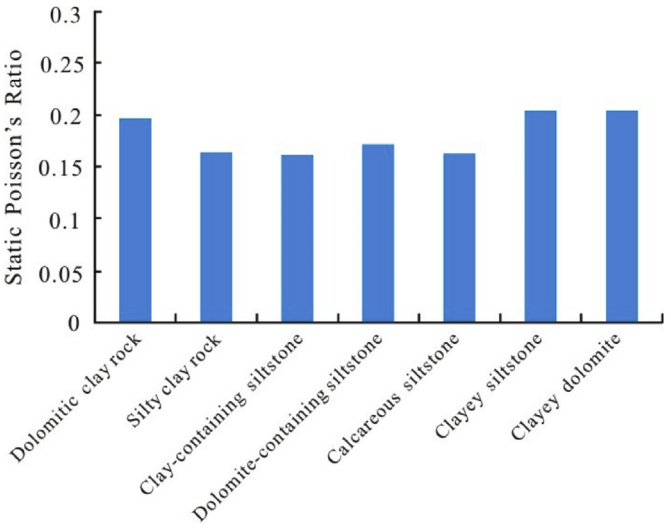

Fig. 7. Static Poisson's ratio of different shale lithologies.

minerals and organic matter were highly plastic, meaning that they have relatively low strength and high plasticity; these characteristics tended to lower rock fracability (Fig. 3). In organic-rich shales, the volume fraction of organic matter (inversely proportional to the Young's modulus and directly proportional to the Poisson's ratio) can be > 30% (Dong et al., 2015); these properties greatly contributed to shale plasticity in our samples (Fig. 4), but are usually neglected. Shales containing abundant felsic and carbonate minerals tended to be brittle and easy to fracture: under stress they developed structural fractures. Brittle components (felsic and carbonate minerals) contained in the shales which developed structural fractures were generally larger than 0.5 (Fig. 5). Therefore, silty and calcareous (dolomitic) lithological successions, which consisted mainly of shale with felsic or carbonate minerals, had higher Young's modulous, lower Poisson's ratios, and higher fracability; clayey lithological successions showed instead the opposite trend (Fig. 6, Fig. 7).

4.2.3. Lithofacies

The analyzed lithofacies demonstrated high fracability when they presented sheet-like or lamellar macrostructures and were mainly composed of felsic or carbonate minerals. Based on our results concerning the Young's modulus and the Poisson's ratio, we can draw two main conclusions (Fig. 8, Fig. 9): (i) the static Young's modulus differs greatly but the Poisson's ratio differs slightly between different lithofacies; (ii) the mineral components had a greater influence than macrostructure on the elastic parameters. Lamellar clayey limestones (dolomite), lamellar clayey siltstones, layered calcareous (dolomitic) siltstones, sheet-like clay-containing siltstones, and flaggy carbonate-containing siltstones all had high Young's modulous and were easily fractured. On the other hand, flaggy calcareous (dolomitic) claystones, layered calcareous (dolomitic) claystones, flaggy silty claystones, layered silty claystones, and sheet-like silty claystones had low static Young's modulous and were difficult to fracture.

4.2.4. Microfractures

The existence of microfractures can change the elastic parameters of a rock (Li et al., 2018). In the studies shales, the occurrence of microfractures lowered the dynamic Young's modulus: this decrease was greater for transverse microfractures than for vertical microfractures (Fig. 10). At the same time, the development of microfractures greatly reduced the rock fracture toughness, lowering the amount of energy needed for rock fracturing and enhancing fracability. Moreover, when a microfracture is filled with carbonate minerals or siliceous minerals, shale brittleness tends to be higher; a condition that favors fracturing. For example, bedding-parallel vein fractures in the studied oil shale

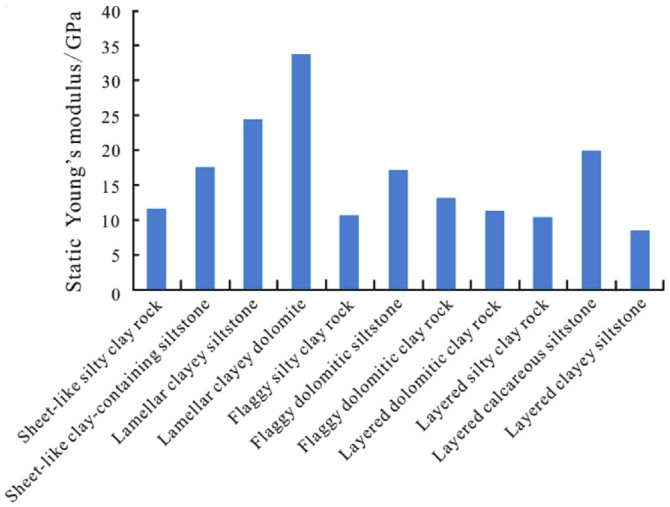

Fig. 8. Static Young's modulus of different shale lithofacies.

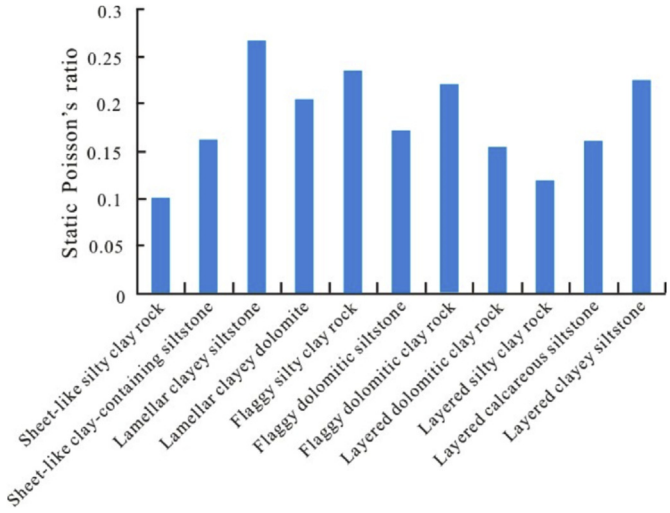

Fig. 9. Static Poisson's ratio of different shale lithofacies.

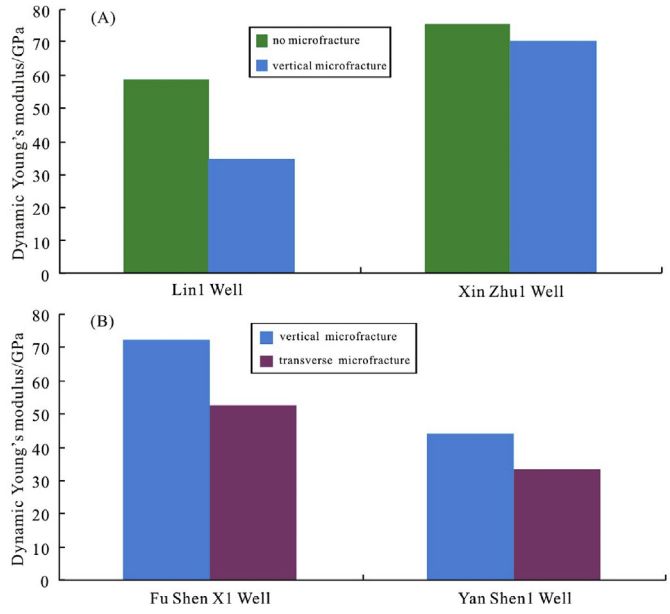

Fig. 10. Influence of microfractures on the dynamic Young's modulus of the shale.

were filled with numerous fibrous calcite veins, which greatly improved fracturing. The analysis of shale fracture mechanics and the true triaxial hydraulic fracturing simulation test showed that the presence of microfractures can favor volume fracturing. Hydraulic fractures tend to cross or change direction when they communicate with microfractures, affecting their extension and shape (Zhao et al., 2012; Zhang et al., 2014; Taleghani et al., 2018). Natural fluid pressure fractures (e.g., bedding-parallel vein fractures, hydrocarbon generation, expulsion fractures) tend to develop horizontally, following the direction of extension of bedding fractures, and to appear in groups. In shale fracturing reconstructions, and in particular during the vertical extension of hydraulic fracturing fractures, it is hence easy to connect multiple groups of natural fluid pressure fractures. This process can result in the formation of fence-shaped and/or network-shaped fractures, and in a significant increase in fracture density (Ma et al., 2016).

4.3. Method for the evaluation of shale fracability

Previous research and our analysis of the factors influencing shale

fracability indicate that rock mineral components and mechanics parameters are the most important parameters affecting shale fracability (Kumar et al., 2018; Xiong et al., 2019). In order to characterize shale fracability, we calculated the brittleness index, based on the mineral components and rock mechanics parameters. Three different formulas can be used to calculate the brittleness index based on mineral components (Equations (4)–(6)).

$$B_{rit} = V_{quartz}/(V_{quartz} + V_{carbonate})*100 \quad (4)$$

$$B_{rit} = V_{felsic}/(V_{felsic} + V_{carbonate})*100 \quad (5)$$

$$B_{rit} = (V_{felsic} + V_{carbonate})/(V_{felsic} + V_{carbonate} + V_{clay})*100 \quad (6)$$

where B_{rit} is the brittleness index, %; V_{quartz} is the content of quartzes, %; $V_{carbonate}$ is the content of carbonate minerals, %; V_{felsic} is the content of felsic minerals, %; V_{clay} is the content of clay minerals, %; $V_{organic}$ is the content of organic matters, %.

The key difference between these methods is the attribution of carbonate minerals. Also note that none of this formulas considers the plasticity of organic matter. We hence constructed a new formula to calculate the brittleness index, which is based on the rock mineral content, but also takes into account the mechanical properties of carbonate minerals and the plastic effect of organic matter (Equation (7)).

$$B_{rit} = (V_{felsic} + V_{carbonate})/(V_{clay} + V_{carbonate} + V_{organic})*100 \quad (7)$$

where B_{rit} is the brittleness index, %; V_{felsic} is the content of felsic minerals, %; $V_{carbonate}$ is the content of carbonate minerals, %; V_{clay} is the content of clay minerals, %; $V_{organic}$ is the content of organic matters, %.

Quartz and feldspar are considered as brittle minerals, clay minerals and organic matter as plastic minerals, and carbonate minerals (e. g, calcite, dolomite) as ductile minerals. The proposed equation has two advantages. The first is that it reflects the dual effect of carbonate minerals on shale fracability: a certain amount of carbonate minerals can increase a rock brittleness, while an excess can increase the strength and fracture toughness of a rock, hindering fracturing transformation. In the actual fracturing process, microfractures usually stopped in the carbonate rocks, which acted as fracturing barriers. The second advantage of the proposed equation is that it considers the effect of organic matter on rock brittleness: when the diagenesis intensity was weak, the content of organic matter was usually high, while the static Young's modulus and Poisson's ratio decreased (Fig. 4). Under such conditions rock brittleness was low; hence, we can conclude that the organic-rich shales had poor fracability.

The rock mechanics parameter method is presently the best for evaluating shale brittleness. In this method, the Young's modulus and the Poisson's ratio are used to calculate the brittleness index; moreover, a weighted summation is performed considering a weight coefficient of 0.5.

Rickman et al. (2008) calculated the brittleness index for the Barnett Shale in the Fort Worth Basin (North America) applying the following equations (8)–(10).

$$E_{Rrit} = (E - 10)/(80 - 10)*100 \quad (8)$$

$$\mu_{Rrit} = (0.4 - \mu)/(0.4 - 0.1)*100 \quad (9)$$

$$B_{rit} = 0.5E_{Rrit} + 0.5\mu_{Rrit} \quad (10)$$

The above calculation method was established based on the rock mechanics parameters of the marine Barnett Shale; hence, it has obvious regional limitations and appropriate parameters should be selected for lithologies located in other regions. In our study area, the dynamic Young's modulus ranged between 24.6 and 75.3 GPa and the dynamic Poisson's ratio between 0.02 and 0.25. The brittleness index could be calculated by following equations (11)–(13).

$$E_{Rrit} = (E - 24.6)/(75.3 - 24.6)*100 \quad (11)$$

$$\mu_{Rrit} = (0.25 - \mu)/(0.25 - 0.02)*100 \quad (12)$$

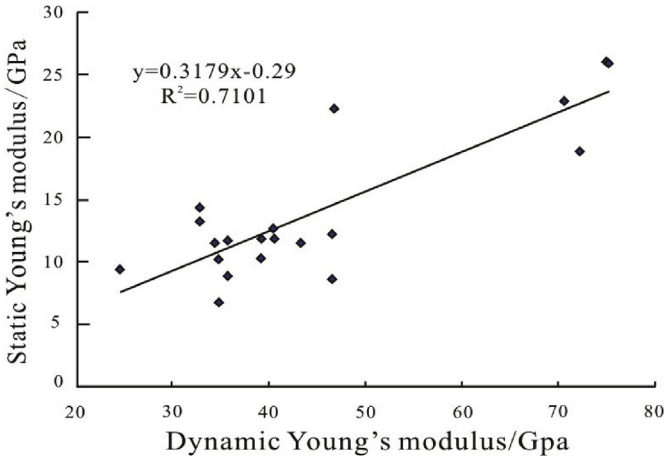

Fig. 11. Relationship between the static Young's modulous and dynamic Young's modulous of the shale.

$$B_{rit} = 0.5E_{Rrit} + 0.5\mu_{Rrit} \quad (13)$$

where E_{Rrit} is the normalized Young's modulus, %; E is the Young's modulus, Gpa; μ_{Rrit} is the normalized Poisson's ratio, %; μ *is* the Poisson's ratio; B_{rit} is the brittleness index, %.

Since the rock mechanics parameters obtained from the P- and S-wave velocities are dynamic, these parameters reflected the rock mechanical properties under instantaneous loading, rather than the long-term static loading under actual conditions. The dynamic and the static Young's modulus values are linked by a good linear relationship, while the dynamic and the static Poisson's ratio values are very similar to each other. Therefore, in practical applications, the dynamic and static Young's modulous can be mutually transformed based on their correlation. In our study area, the dynamic and static Young's modulus values were linked by a good linear relationship: the former values were 2–3 times higher than the latter values (Fig. 11).

The brittleness indices calculated for the same lithofacies, obtained by the mineral component and rock mechanics parameters methods, presented a good linear correlation (Fig. 12); hence, the mineral component method (Equation (7)) proposed in this paper seems appropriate for the evaluation of shale brittleness. This method has a good

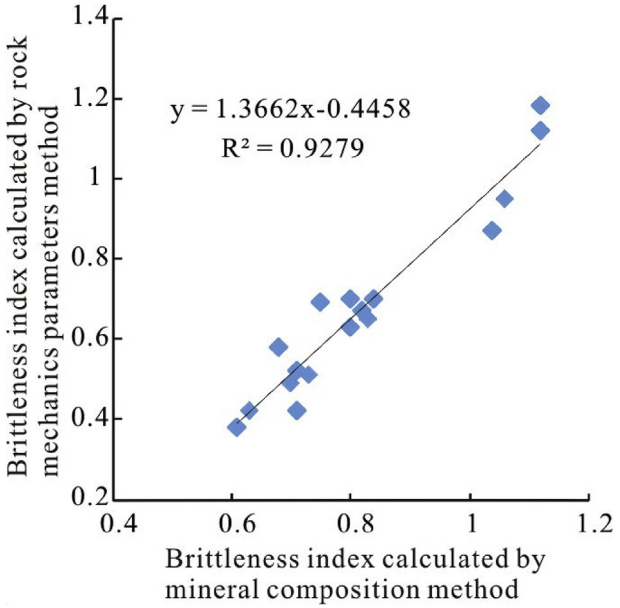

Fig. 12. Comparison between the brittleness indices calculated by the mineral component and the rock mechanics parameters method.

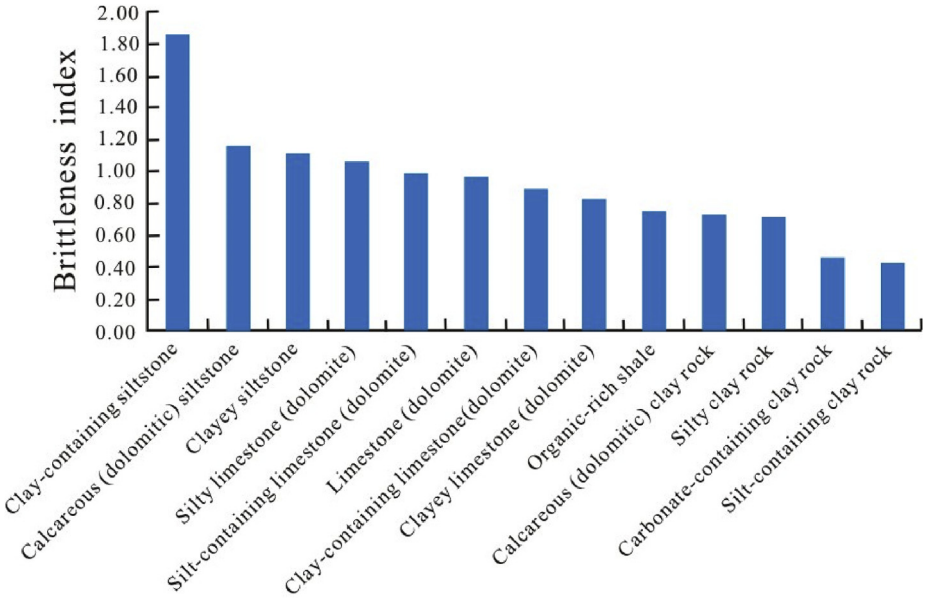

Fig. 13. Brittleness indices of different shale lithofacies.

application value in areas where rock mechanics test or array acoustic logging data are lacking.

The results obtained from the mineral components method and the statistical analysis of the shale brittleness indices demonstrate that a higher carbonate mineral content corresponded lower brittleness in the silty lithological successions, but to higher brittleness in the clayey and organic-rich lithological successions. In other words, the silty lithological successions were the most easy to fracture in shales, followed by the calcareous (dolomitic), and the clayey or organic-rich lithological successions (Fig. 13).

5. Conclusion

Rock components are key factors affecting shale fracability. On one hand, shales with sheet-like and lamellar structures are more easily fractured; on the other hand, carbonate minerals have strong fracture toughness. Appropriate amounts of carbonate minerals can increase a rock brittleness, while an excess will enhance its cohesion, rendering fracturing transformations more difficult. Felsic minerals have high brittleness (which favors fracturing transformations), while clay minerals and organic matter have strong plasticity (which hinders fracturing transformations). The presence of microfractures reduces rock fracture toughness and enhances rock fracability. Overall, the influence of rock components determines the high fracability of lamellar clayey limestones (dolomites), lamellar clayey siltstones, layered calcareous (dolomitic) siltstones, sheet-like clay-containing siltstones, and flaggy carbonate-containing siltstones.

According to the mechanical properties of carbonate minerals and the plastic effect of organic matter, we proposed a new formula for the calculation of the brittleness index, which is based on the mineral component method. The brittleness index values calculated through the proposed formula have a good linear correlation with those obtained through the rock mechanics parameters method. The brittleness indices showed that the silty lithological successions were the most easy to fracture in shales, followed by the calcareous (dolomitic), ad clayey or organic-rich lithological successions.

Acknowledgements

This work was supported by the Natural Science Foundation of China (Grant No. 41802172; 41830431), the National Science, Technology Major Project, P. R. China (Grant No. 2017ZX05009-001), the Natural Science Foundation of Shandong Province (Grant No. ZR2018BD014), the China Postdoctoral Science Foundation (Grant No. 2018M632742), and the Fundamental Research Funds for the Central Universities (Grant No. 18CX02178A).

References

Andreev, G.E., 1995. Brittle Failure of Rock Materials. CRC Press.
Beugelsdijk, L.J.L., De Pater, C.J., Sato, K., 2000. Experimental hydraulic fracture propagation in a multi-fractured medium. In: SPE Asia Pacific Conference on Integrated Modelling for Asset Management. SPE 59419, pp. 1–8.
Bishop, A.W., 1967. Progressive failure with special reference to the mechanism causing it. In: Oslo: Proceedings of the Geotechnical Conference, pp. 142–150.
Breyer, J.A., Alsleben, H., Enderlin, M.B., 2010. Predicting fracability in shale reservoirs. In: AAPG Search and Discovery Article, AAPG Hedberg Conference, Austin, Texas.
Chekhonin, E., Popov, E., Popov, Y., Gabova, A., Romushkevich, R., Spasennykh, M., Zagranovskaya, D., 2018. High-resolution evaluation of elastic properties and anisotropy of unconventional reservoir rocks via thermal core logging. Rock Mech. Rock Eng. 51 (9), 2747–2759.
Chong, K.K., Grieser, W.V., Passman, A., Tamayo, H.C., Modeland, N., Burke, B.E., 2010. A completions guide book to shale-play development: a review of successful approaches toward shale-play stimulation in the last two decades. In: Proceedings of Canadian Unconvetional Resources and International Petroleum Conference, 19-21 October, Calgary, Alberta, Canada: CSUG/SPE, 2010, SPE 133874.
Deng, J.Y., Chen, Z.R., Geng, Y.N., Liu, S.J., Zhu, H.Y., 2013. Prediction model for in-situ formation stress in shale reservoirs. J. China Univ. Pet. 37 (6), 59–64.
Dong, C.M., Ma, C.F., Lin, C.Y., Sun, X., Yuan, M.Y., 2015. A method of classification of shale set. J. China Univ. Pet. 39 (3), 1–7.
Goodway, B., Perez, M., Varsek, J., Abaco, C., 2010. Seismic petrophysics and isotropic-anisotropic AVO methods for unconventional gas exploration. Lead. Edge 29 (12), 1500–1508.
Gui, R., Wang, Y.P., 2012. Rock mechanics parameter calculation based on conventional logging data: a case study of upper paleozoic in ordos basin. J. Geomechanics 18 (4), 418–424.
Guo, H.X., Guo, T.K., 2013. Experimental evaluation of crushability of shale reservoirs in luojia area,shengli oilfield. Pet. Geol. Exp. 35 (3), 339–346.
Hajiabdolmajid, V., Kaiser, P., 2003. Brittleness of rock and stability assessment in hard rock tunneling. Tunn. Undergr. Space Technol. 18 (1), 35–48.
Hao, Y.Q., Song, G.Q., Zhou, G.Q., Li, Z., Wang, W.Q., Li, B., Zhang, C.X., 2016. Influence of petrological characteristics on fracability of the paleogene shale, jiyang depression. Pet. Geol. Exp. 38 (4), 489–495.
Honda, H., Sanada, Y., 1956. Hardness of coal. Fuel 35 (4), 451–461.
Hucka, V., Das, B., 1974. Brittleness determination of rocks by different methods. In: International Journal of Rock Mechanics and Mining Sciences & Geomechanics Abstracts, vol. 11. Elsevier, pp. 389–392.
James, J., Bo, H., 2007. Lithofacies summary of the Mississippian Barnett Shale,Mitchell 2 T.P. Sims well,Wise County, Texas. AAPG Bull. 91 (4), 437–443.
Jarvie, D.M., Hill, R.J., Ruble, T.E., Pollastro, R.M., 2007. Unconventional shale-gas systems: The Mississippian Barnett Shale of north-central Texas as one model for thermogenic shale-gas assessment. AAPG Bull. 91 (4), 475–499.
Jin, X., Shah, S.N., Roegiers, J.C., Zhang, B., 2014. Fracability evaluation in shale

reservoirs-an integrated petrophysics and geomechanics approach. SPE J. 20 (3), 518–526.
Kivi, I.R., Ameri, M., Molladavoodi, H., 2018. Shale brittleness evaluation based on energy balance analysis of stress-strain curves. J. Pet. Sci. Eng. 167, 1–19.
Kumar, S., Das, S., Bastia, R., Ojha, K., 2018. Mineralogical and morphological characterization of older Cambay shale from north Cambay basin, India: implication for shale oil/gas development. Mar. Pet. Geol. 97, 339–354.
Lawn, B.R., Marshall, D.B., 1979. Hardness, toughness, and brittleness: an indentation analysis. J. Am. Ceram. Soc. 62 (7–8), 347–350.
Li, J.Y., 2013. Analysis on mineral components and frangibility of shales in dongying depression. Acta Sedimentol. Sin. 31 (4), 616–620.
Li, Z., Li, L., Li, M., Zhang, L., Zhang, Z., Huang, B., Tang, C.A., 2018. A numerical investigation on the effects of rock brittleness on the hydraulic fractures in the shale reservoir. J. Nat. Gas Sci. Eng. 50, 22–32.
Liu, Z.S., Sun, Z.D., 2015. New brittleness indexes and their application in shale/clay gas reservoir prediction. Petrol. Explor. Dev. 42 (1), 129–137.
Ma, C.F., Dong, C.M., Luan, G.Q., Lin, C.Y., Liu, X.C., Elsworth, D., 2016. Types,characteristics and effects of natural fluid pressure fractures in shale:a case study of the paleogene strata in eastern China. Petrol. Explor. Dev. 43 (4), 580–589.
Mohamed, O., Roger, M., 2012. Lithofacies and sequence stratigraphy of the Barnett shale in east-central Fort Worth Basin, Texas. AAPG Bull. 96 (1), 1–22.
Mullen, M., Enderlin, M., 2012. Fracability Index-more than just calculating rock properties, SPE 159755. In: Paper 159755-MS Presented at the SPE Annual Technical Conference and Exhibition. San Antonio, Texas, USA, pp. 10–11.
Oyler, D.C., Mark, C., Molinda, G.M., 2010. In situ estimation of roof rock strength using sonic logging. Int. J. Coal Geol. 83 (4), 484–490.
Quinn, J.B., Quinn, G.D., 1997. Indentation brittleness of ceramics: a fresh approach. J. Mater. Sci. 32 (16), 4331–4346.
Rickman, R., Mullen, M.J., Petre, J.E., Grieser, W.V., Kundert, D., 2008. A practical use of shale petrophysics for stimulation design optimization: all shale plays are not clones of the Barnett Shale. In: SPE Annual Technical Conference and Exhibition.
Sheng, Q.H., Li, W.C., 2016. Evaluation method of shale fracability and its application in jiaoshiba area. Prog. Geophys. 31 (4), 1473–1479.
Taleghani, A.D., Gonzalez-Chavez, M., Yu, H., Asala, H., 2018. Numerical simulation of hydraulic fracture propagation in naturally fractured formations using the cohesive zone model. J. Pet. Sci. Eng. 165, 42–57.
Tang, Y., Xing, Y., Li, L.Z., Zhang, H.B., Jiang, S.X., 2012. Influence factors and evaluation methods of the gas shale fracability. Earth Sci. Front. 19 (5), 356–363.
Tissot, B.P., Welte, D.H., 1978. Petroleum Formation and Occurrence. Springer-Verlag, New York.
Wang, F.P., Gale, J.F.W., 2009. Screening criteria for shale-gas systems. Gulf Coast Assoc. Geol. Soc. Trans. 59, 779–793.
Wang, G.H., Timothy, R.C., 2013. Organic-rich Marcellus Shale lithofacies modeling and distribution pattern analysis in the Appalachian Basin. AAPG Bull. 97 (12), 2173–2205.
Wang, G.M., 2012. Laminae combination and genetic classification of Eogene shale in Jiyang depression. J. Jilin Univ. (Earth Sci. Ed.) 42 (3), 666–671.
Wu, J., Zhang, S., Cao, H., Zheng, M., Sun, P., Luo, X., 2018. Fracability evaluation of shale gas reservoir-A case study in the Lower Cambrian Niutitang formation, northwestern Hunan, China. J. Pet. Sci. Eng. 164, 675–684.
Wu, T., 2015. Study on Influencing Factors and Evaluation Method of Rock Brittleness in Shale Gas Layer. Cheng Du, Southwest Petroleum University, pp. 1–87.
Xiong, Z., Wang, G., Cao, Y., Liang, C., Li, M., Shi, X., Zhang, B., Li, J., Fu, Y., 2019. Controlling effect of texture on fracability in lacustrine fine-grained sedimentary rocks. Mar. Pet. Geol. 101, 195–210.
Yasin, Q., Du, Q., Sohail, G.M., Ismail, A., 2017. Impact of organic contents and brittleness indices to differentiate the brittle-ductile transitional zone in shale gas reservoir. Geosci. J. 21 (5), 779–789.
Yuan, J., Zhou, J., Liu, S., Feng, Y., Deng, J., Xie, Q., Lu, Z., 2017. An improved fracability-evaluation method for shale reservoirs based on new fracture toughness-prediction models. SPE J. 22 (5), 1–10.
Yuan, J.L., Deng, J.Y., Zhang, D.Y., Li, D.H., Yan, W., Chen, Z.G., Cheng, L.J., Chen, Z.J., 2013. Fracability evaluation of shale-gas reservoirs. Acta Pet. Sin. 34 (3), 523–527.
Zhang, S.C., Guo, T.K., Zhou, T., Zou, Y.S., Mu, S.R., 2014. Fracture propagation mechanism experiment of hydraulic fracturing in natural shale. Acta Pet. Sin. 35 (3), 496–503 518.
Zhao, H.F., Chen, M., Jin, Y., Ding, Y.H., Wang, Y.H., 2012. Rock fracture kinetics of the facture mesh system in shale gas reservoirs. Petrol. Explor. Dev. 39 (4), 498–503.
Zhao, J.Z., Xu, W.J., Li, Y.M., Hu, J.Y., Li, J.Q., 2015. A new method for fracability evaluation of shale-gas reservoirs. Nat. Gas Geosci. 26 (6), 1165–1172.
Zhao, J.Z., Yi, Q., Li, Y.M., 2017. Key scientific issues of hydraulic fracturing in Chinese shale gas reservoir. Sci. Sin. 47 (11), 19–32.
Zhou, H., Meng, F.Z., Zhang, C.Q., Xu, R.C., Lu, J.J., 2014. Quantitative evaluation of rock brittleness based on stress-strain curve. Chin. J. Rock Mech. Eng. 33 (6), 1114–1122.
Zhuang, Z., Liu, Z.L., Wang, T., Gao, Y., Wang, Y.H., Fu, H.F., 2016. The key mechanical problems on hydraulic fracture in shale. Chin. Sci. Bull. 61 (1), 72–81.